DOI 10.4430/bgo00402

Application of instantaneous amplitude and spectral decomposition to determine the location and thickness of a hydrocarbon reservoir

M. Rahimi[1,2] and M.A. Riahi[2]

[1] *Faculty of Earth Sciences, Shahid Chamran University of Ahvaz, Ahvaz, Iran*
[2] *Institute of Geophysics, University of Tehran, Tehran, Iran*

(Received: 23 April 2022; accepted: 19 July 2022; published online: 16 November 2022)

ABSTRACT Spectral decomposition is a robust attribute in the characterisation of post-stack seismic data. Reflected wavelets from specific geological lithologies show distinct patterns in the frequency spectrum, which is related to the wavelet frequency content and the interference pattern of a structure within a layer. Generally, the frequency spectrum of a wavelet has a smooth pattern through the entire bandwidth. However, the structure of a layer, such as its thickness and lateral distribution, will appear as a periodic function in the frequency domain. This research investigates the distinct patterns of reflective layers with different thicknesses using instantaneous amplitude and fast sparse S-transform (ST). To verify the efficiency of both methods, we have examined these approaches on channel-shaped and wedge-shaped synthetic models. The results showed that the fast sparse ST could predict features of both synthetic models better than the instantaneous amplitude. Next, the fast sparse ST is performed on experimental field data selected from a time interval containing a hydrocarbon channel reservoir. We used a sparse deconvolution algorithm to suppress the wavelet effect and balance all the frequencies. The results of this research showed the efficiency of the fast sparse ST in predicting a hydrocarbon channel reservoir's thickness.

Key words: channel detection, fast sparse S-transform, frequency analysis, instantaneous amplitude, seismic attribute.

1. Introduction

Spectral decomposition of seismic data provides robust interpretation tools for hydrocarbon investigation and thickness estimation by analysing attenuation effects (Luo *et al*., 2020; Oluwadare *et al*., 2020). This is especially important for hydrocarbon reservoir characterisation in carbonate environments. In seismic interpretation, spectral decomposition refers to any method that produces a continuous time-frequency analysis of seismic information. Thus, a frequency spectrum is output for each time sample of the seismic trace. Spectral decomposition has been used for a variety of applications including layer thickness determination (Partyka *et al*., 1999; Othman *et al*., 2016; Guo *et al*., 2020; Zhou *et al*., 2021), stratigraphic visualisation (Marfurt and Kirlin, 2001; Ehirim and Akpan, 2017), and direct hydrocarbon detection (Castagna *et al*., 2003; Chopra and Marfurt, 2007). Spectral decomposition is a non-unique process, thus, a single seismic trace can produce various time-frequency analyses.

Spectral decomposition of an input seismic trace refers to methods that compute the spectral-

magnitude and spectral-phase components at every frequency sample (Allen and Rabinar, 1977; Badly, 1985; Chakraborty and Okaya, 1995; Chopra and Marfurt, 2006). Liu (2006) showed that images produced from spectral decomposition are well-correlated with the layer thickness. Widess (1973) showed the approximate linear variation of the amplitudes with layer intervals less than the tuning thickness. Chuang and Lawton (1995) generalised this work to a frequency spectrum and observed that the peak frequency slightly increased with decreasing layer thickness. The repetition frequency pattern in frequency spectra of the seismic data denotes the higher resolution of the reservoir zone. This qualitative aspect of the frequency spectrum can be used as an attribute. In this research, the instantaneous amplitude is used to identify bright spots as an effective tool to detect gas accumulations. The premise of the current research is obtaining resolution reliability using instantaneous amplitude and spectral decomposition. This process provides promising reservoir properties necessary for characterisation purposes.

This study investigates the Asmari Formation of the giant Marun Oilfield located in the Dezful Embayment, SW Iran. The Marun Oilfield was discovered by seismic data, and an exploration well was drilled in 1963, this oilfield has a north-western to south-eastern asymmetrical anticline. This investigation uses seismic attribute analysis including instantaneous amplitude and spectral decomposition of the Asmari Formation. Seismic attributes typically provide information relating to the seismic data reflection's amplitude, geometry and position. Seismic attribute analysis is able to extract information from seismic data that is otherwise hidden in the data and this method is used to identify depositional environments (e.g. fluvial or deep-water channels), and even provide direct hydrocarbon indicators. The seismic attribute analysis serves as the interpreter, augmenting the geological interpretation of a formation, particularly in the thin-bed reservoir area. In seismic reservoir characterisation, it is important to use proper attributes to delineate its structure and other properties. The seismic attributes can reveal several characteristics of a hydrocarbon reservoir, which are not visually visible in the stacked section. In this research, the seismic attribute analysis showed evidence of subaerial exposure and a channel system near the Asmari and Gachsaran formations, which may be considered the carbonate sequence boundary (Van Buchem *et al*., 2010; Ashtari and Arzani 2016). The geological studies estimated the presence of the channel shape reservoir in the studied area. The seismic attribute analysis was performed to verify this geological feature estimation in this reservoir environment. The investigation shows how spectral decomposition assists in verifying geological predictions.

We begin with a brief introduction of the two methodologies used in this study, followed by the analysis and examining the results of synthetic modelling. Next, we introduce experimental field data and the related geology. Finally, after applying the methods to the experimental field data set, we compared the seismic attributes' analysis results.

2. Methodology

In this study, an attempt was made to evaluate the relation between reflector thickness and frequency spectra. Instantaneous amplitude attributes can be used to determine reservoir intervals based on thickness variations. Detailed explanations about seismic attributes are presented by Tanner *et al*. (1979). The instantaneous amplitude attribute presents a combination of real and quadrature components considered a complex seismic trace. The channel reservoir data will be investigated by spectral decomposition using the instantaneous amplitude attribute (Zheng *et al*., 2007; Zeng, 2010; Yan *et al*., 2018). In the next step, fast sparse S-transform [ST: Sattari (2017)] is used to enhance the capacity of Spectral Decomposition at different depths

The current study was conducted with the generated 3D seismic cube from 2D survey data for an offshore oilfield.

2.1. Instantaneous amplitude

Synthetic and real seismic data were used to evaluate the effectiveness of both instantaneous and spectral decomposition attributes in detecting channel-shaped reservoirs.

2.1.1. Synthetic example

A schematic representation of the layered 3D Earth model, consisting of two-channel reservoirs at different depths and locations with desired orientations, is displayed in Fig. 1. This figure displays a three-dimensional synthetic layered model consisting of two-channel reservoirs at different time depths with desired positions and orientations. An in-line and cross-line representation of this synthetic model is normal incidence data, which is displayed in Figs. 2 and 3. The wavelet type is the Ricker wavelet with a 20 Hz peak frequency.

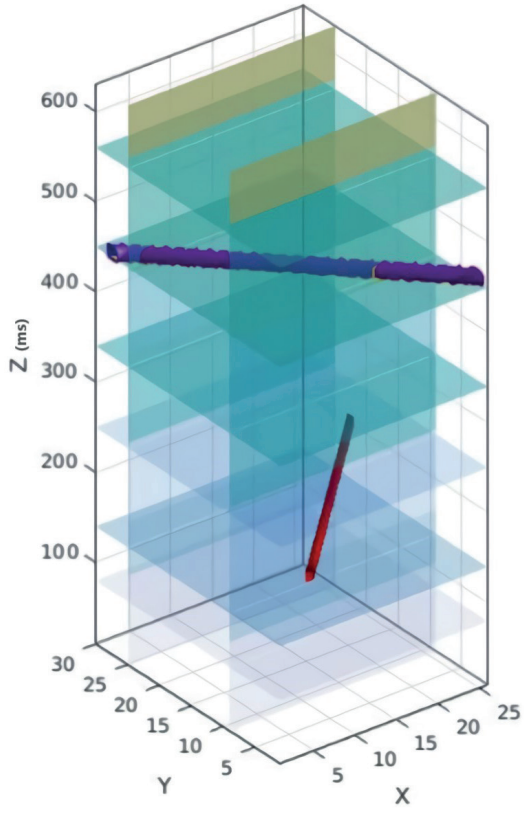

Fig. 1 - Schematic representation of 3D Earth model layered consisting of two - channel reservoirs with different depths, locations, and orientations.

A two-dimensional representation of in-line and cross-line of introduced synthetic data (Fig. 1) is shown in Figs. 2 and 3.

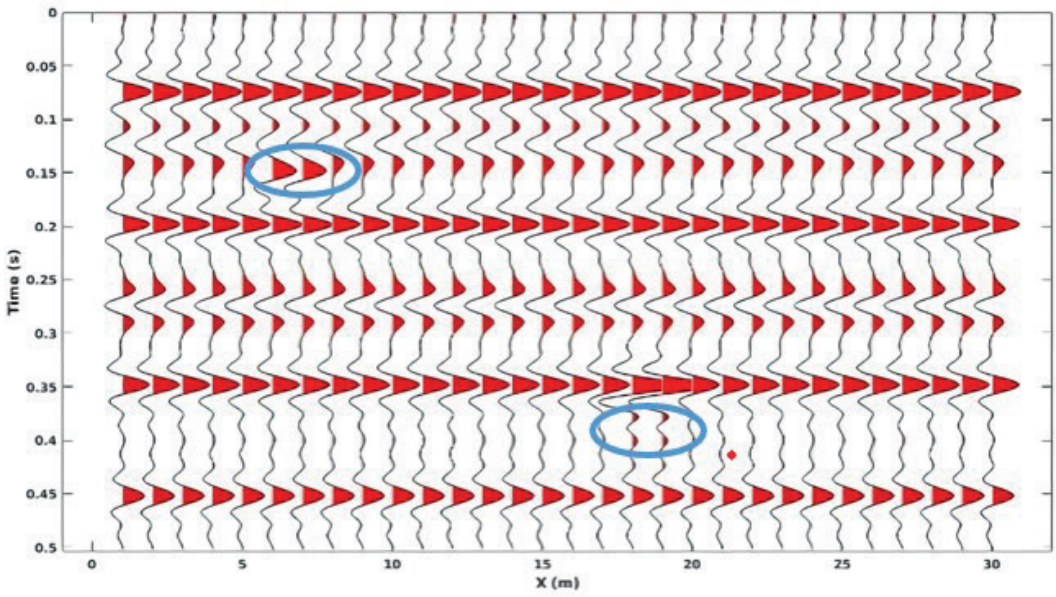

Fig. 2 - The 2D in-line section was extracted from a 3D synthetic model (Fig. 1). This section shows that the locations of the buried channels, marked by blue ellipsoids, are unclear.

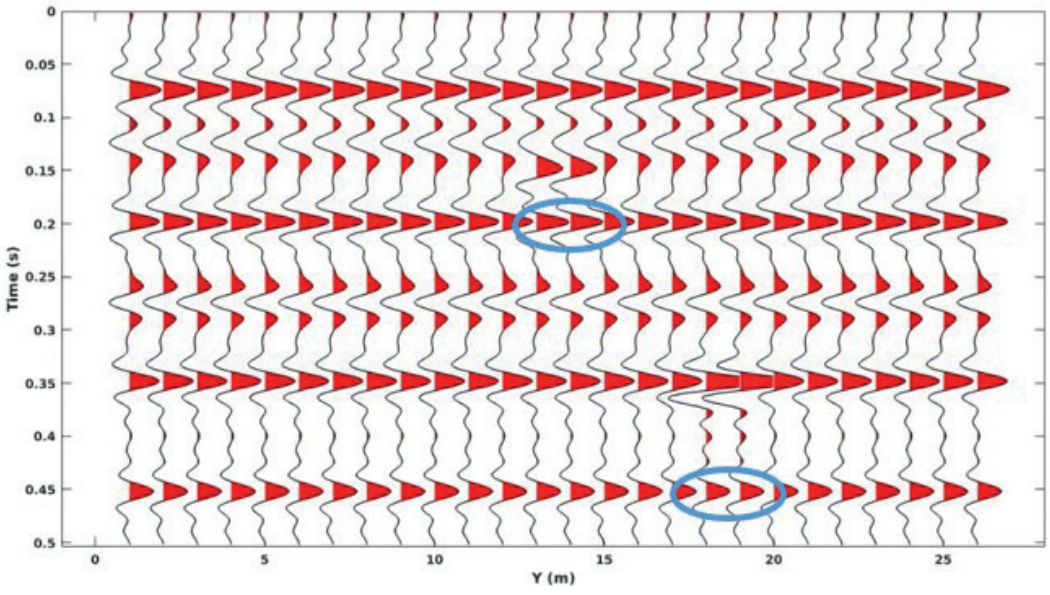

Fig. 3 - The 2D cross-line section was extracted from a 3D synthetic model (Fig. 1). This section shows that the locations of the buried channels, marked by blue ellipsoids, are unclear.

The data are now used as the input for seismic attribute modules by a single-channel sparse deconvolution method (Jeong *et al.*, 2013). 2D in-line and cross-line representations of deconvolved data are shown in Figs. 4 and 5.

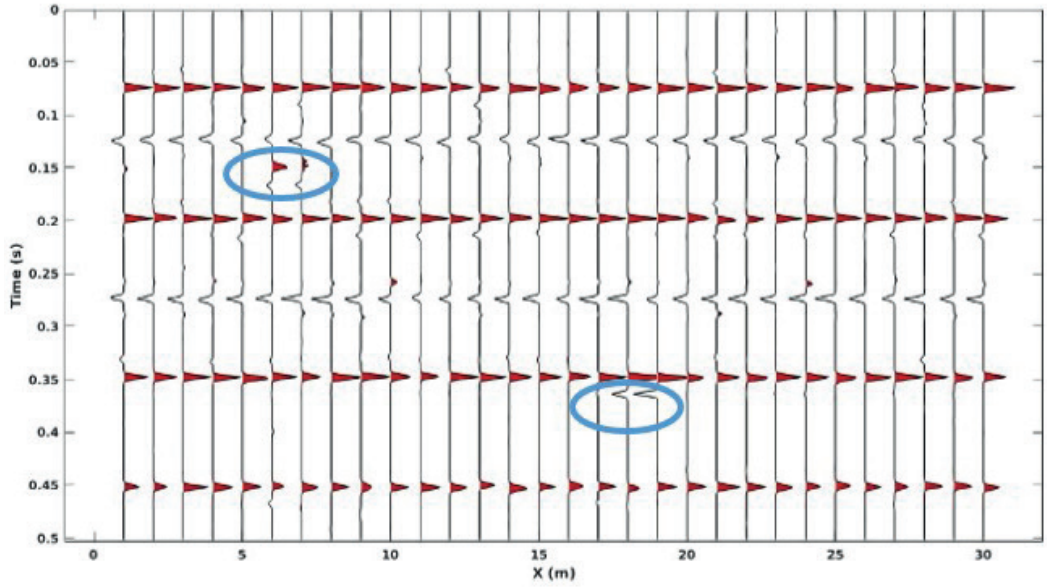

Fig. 4 - The 2D in-line section after applying sparse deconvolution on the synthetic data of Fig. 2. The seismic section represents the algorithm performance of space deconvolution.

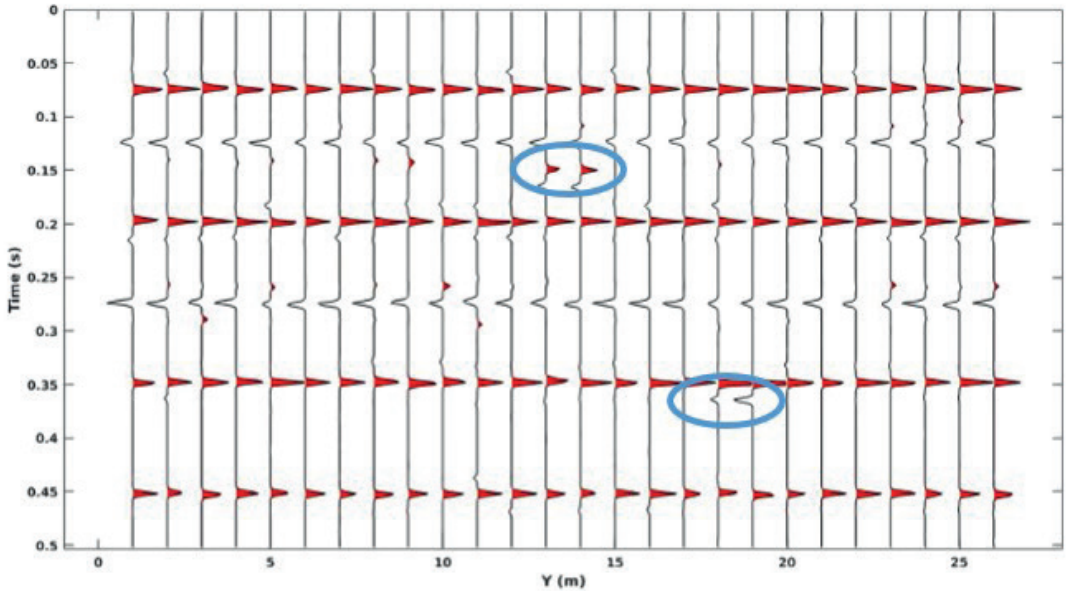

Fig. 5 - The 2D cross-line section after applying sparse deconvolution on the synthetic data of Fig. 3. The seismic section represents the algorithm performance of space deconvolution.

To select the boundary of channels within the reservoir, instantaneous amplitude attributes are used (Jeong *et al*., 2013). Different methods are proposed to calculate a seismic attribute (amplitude, phase, frequency), including quantity extracted, and seismic data-driven (Barnes,

1993, 2007). A seismic trace $f(t)$ can be expressed as the product of instantaneous amplitude $A(t)$ and the cosine of instantaneous phase $\theta(t)$:

$$f(t) = A(t)cos\theta(t) \quad (1)$$

Eq.1 has one known variable [i.e. $f(t)$], and two unknown variables, $A(t)$ and $\theta(t)$. Tanner *et al*. (1979) introduced complex trace analysis to resolve this problem.

The complex trace attributes are derived from the analytic signal as a powerful tool for computing instantaneous attributes. Analytic trace analysis assumes a seismic trace $f(t)$ as a real part of a complex trace:

$$F(t) = f(t) + if^*(t) \quad (2)$$

The imaginary component $f^*(t)$ is ascertained from the real component. A real component can be expressed as the time-dependent amplitude $A(t)$ and time-dependent phase $\theta(t)$. Taking:

$$f(t) = A(t)cos\theta(t)$$

and

$$f^*(t) = A(t)sin\theta(t)$$

giving $f(t)$ and $f^*(t)$ the solution to $A(t)$ and Q(t) is straightforward:

$$A(t) = \sqrt{[f(t)]^2 + [f^*(t)]^2} \quad (3)$$

$$\theta(t) = tan^{-1}\left[\frac{f^*(t)}{f(t)}\right] \quad (4)$$

This attribute is sensitive to high-amplitude variations in the reservoir channel region. Then, it is applied to the 3D convolved data. A 2D time slice image for each seismic trace is used to demonstrate the proper output result. Time slices at t_1 = 0.15 and t_2 = 0.4 ms, shown in Figs. 6 and 7, correspond to the channel-shaped hydrocarbon reservoir.

To determine the reservoir location in time using instantaneous amplitude attributes, the first step is to analyse the frequency content of the data. For this purpose, data are separated by time intervals Dt = 0.1 ms, therefore, we select the time interval of 0.1 ms for the frequency analysis.

These data are considered as the input of the analytical frequency attribute. Time slices at the upper and lower levels of the target reservoir are between 0.15-0.16 and 0.4-0.41 ms, respectively. The method is then followed by the frequency attributes analysis. The attributes analysis of frequency is employed for the upper reservoir boundary (i.e. 0.15-0.16 ms) using a 20 Hz frequency interval. Frequency analysis attributes qualities are superior to instantaneous attributes. They are also less noise-sensitive. 15-Hz-level frequency-related outputs are shown

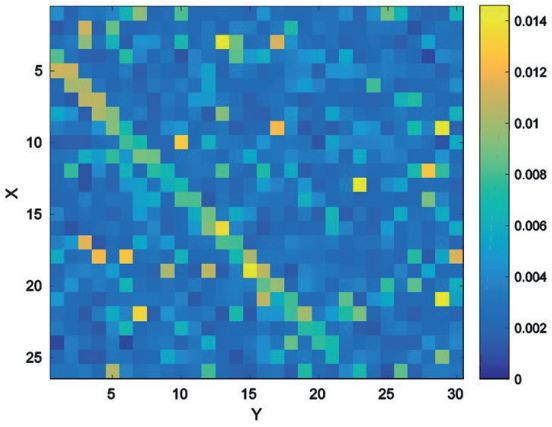

Fig. 6 - Time-slice (0.15 ms above reservoir) obtained from instantaneous amplitude. The oblique pixels show the trace of the upper channel-shaped reservoir in the synthetic model (Fig. 1).

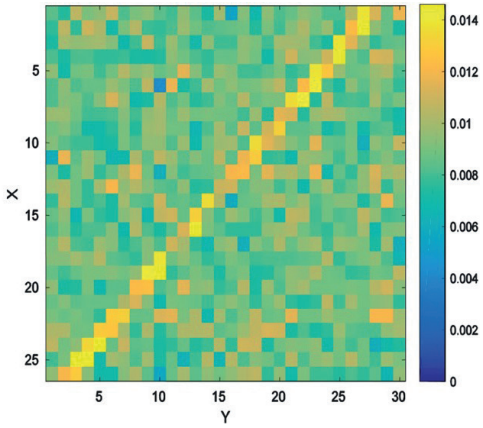

Fig. 7 - Time-slice (0.4 ms below reservoir) obtained from instantaneous amplitude. The oblique pixels show the trace of the lower channel-shaped reservoir in the synthetic model (Fig. 1).

in Figs 8 and 9. As can be seen from these figures, the reservoir area thickness and time interval are correctly determined.

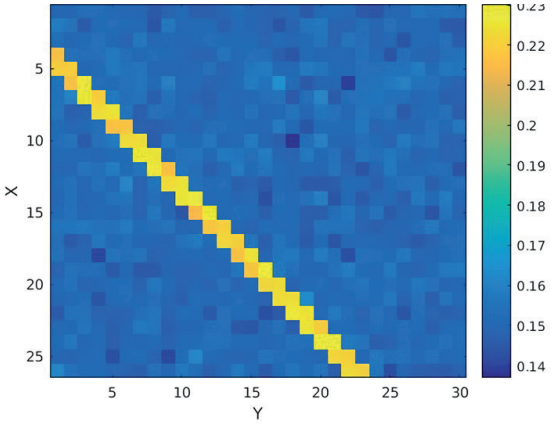

Fig. 8 - Frequency analysis attribute results correspond to the upper channel-shaped reservoir boundary for 0.15-0.16 ms and 20 Hz frequency. As can be noted from this figure, the thickness and time interval of the channel-shaped reservoir area are correctly determined.

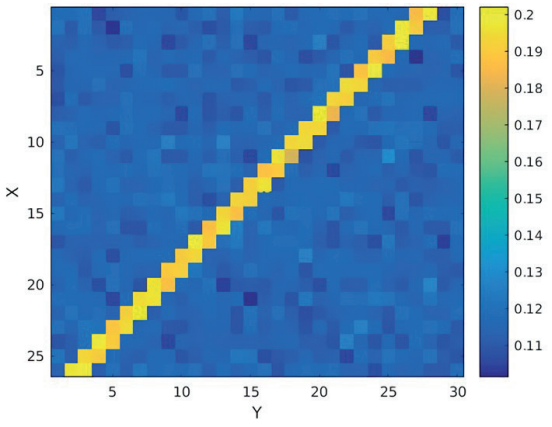

Fig. 9 - The frequency analysis attribute corresponds to a lower channel-shaped reservoir boundary for 0.4-0.41 ms and 20 Hz frequency. As can be seen, the thickness and time interval of the channel-shaped reservoir area are correctly determined.

2.2. Fast sparse S-transform

This method is robust due to reducing uncertainty in the time-frequency panels leading to an increased resolution in both time and frequency. In this method, a novel Sparsity-Based window parameter optimisation (Bourguignon *et al*., 2007) is proposed with which the sparse ST is supplemented to satisfy the need for regularising the sudden frequency variations and stabilising

the results. The applied advanced procedure was helpful to tackle seismic phenomena such as multiple thin-bed layers (Raef *et al.*, 2017). This method has shown high performance as compared with previous methods such as sparse Short-Time Fourier Transform (STFT) because the new algorithm is applied on both time and depth domains simultaneously. Although it is considered a major discovery when the ST was proposed (Stockwell, 2007), it is nonetheless similar to the STFT (Gabor, 1946). Let $x(t) \in$ RN be the objective trace whose time-frequency representation is desired using the time definition of ST (Sattari, 2017).

We perform the time-frequency sparse ST (Sattari, 2017) on all seismic traces. Since the sparse ST in the time-frequency space is sparser than the conventional ST (Stockwell, 2007), the uncertainty in time and frequency is, therefore, less than the conventional ST. This means that the local frequency behaviour at a different time is better detectable and distinguishable (Sattari, 2017). Fig. 10 shows the time-frequency transform of one of the seismic traces selected from the 3D cube ST.

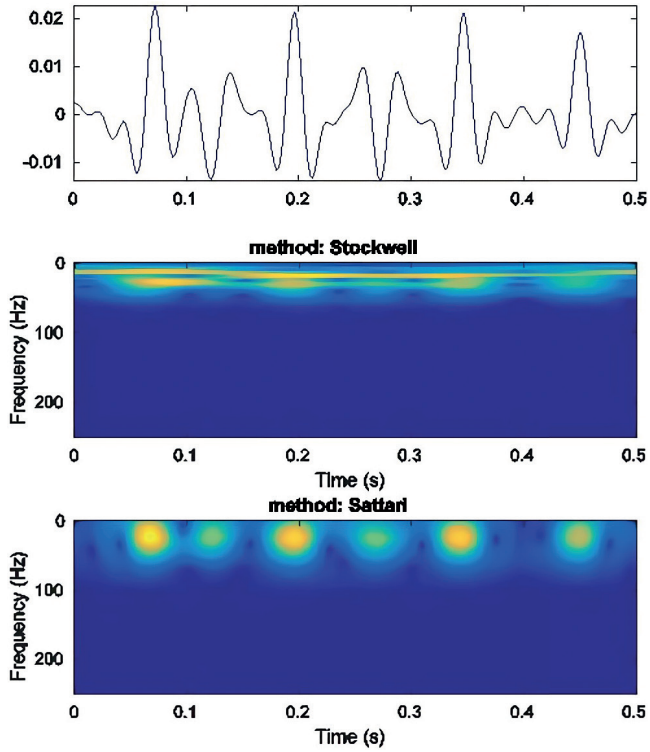

Fig. 10 - Time-frequency transform of one of the seismic traces selected from the 3D cube: a) seismic traces selected from the 3D cube; b) time-frequency transform using conventional ST (Stockwell, 2007); c) time-frequency transform using sparse ST (Sattari, 2017). Of note, the time-frequency frequency image performed by sparse ST (Fig. 10c) shows a better resolution than the conventional ST (Fig. 10b).

The seismic trace shown in Fig. 10a is used as an input for seismic single-channel sparse deconvolution (Jeong *et al.*, 2013). Then, both conventional and sparse ST were performed on the deconvolved trace (Fig. 11a). It is notable that the time-frequency frequency image performed by the sparse ST (Fig. 11c) shows a better resolution than the conventional ST (Fig. 11b).

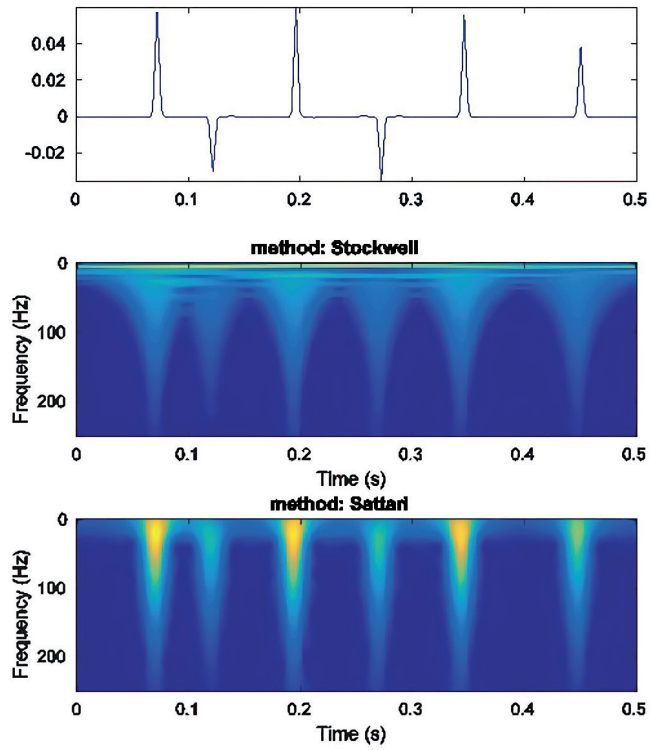

Fig. 11 - Time-frequency transform of one of the deconvolved seismic traces selected from the 3D cube: a) deconvolved seismic trace selected from the 3D cube; b) time-frequency transform using conventional ST (Stockwell, 2007); c) time-frequency transform using sparse ST (Sattari, 2017). Note the time-frequency frequency image performed by sparse ST (Fig. 11c) shows a better resolution than the conventional ST (Fig. 11b).

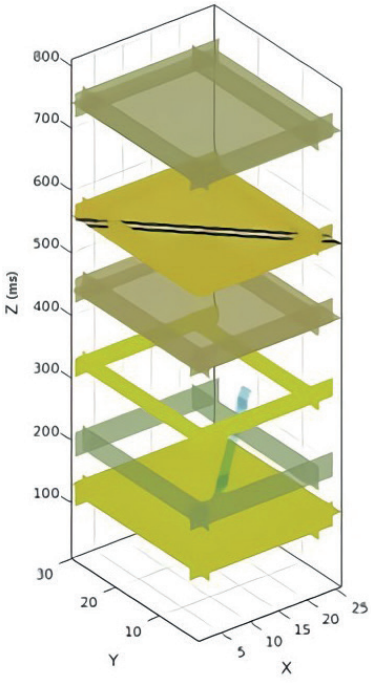

Fig. 12 - The 3D Earth model consists of two channel-shaped reservoirs having different depths, locations, and orientations obtained by employing fast sparse ST on the synthetic model (Fig. 1).

Concerning the acceptable result obtained in Fig. 11c, we perform the time-frequency using sparse ST for the whole cube (Fig. 1). Fig. 12 shows the results obtained from sparse ST; note that the location of the channel-shaped reservoirs is properly constrained. This model represents a layered 3D Earth model consisting of two channel-shaped reservoirs having different depths, locations, and orientations. As can be seen, Fig. 12 shows that the result is in good agreement with the starting model (Fig. 1) in detecting two channel-shaped target reservoirs.

2.3. Wedge model

To compare the precision and efficiency of the fast sparse ST (Sattari, 2017) with the conventional ST proposed by Stockwell (2007) a wedge shape including a thin sand reservoir is considered (Fig. 13). The reflection coefficient of the top and bottom of the thin layer is identical with opposite polarity. We have used a Ricker wavelet with various frequencies to investigate its effect on the resulting frequency analysis.

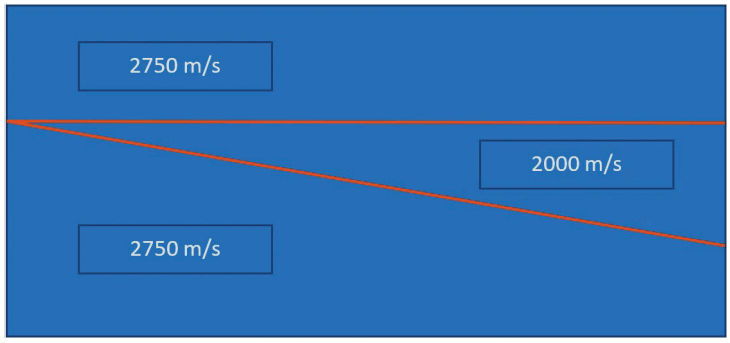

Fig. 13 - A homogeneous synthetic model to test the efficiency of conventional ST and the fast sparse ST, respectively.

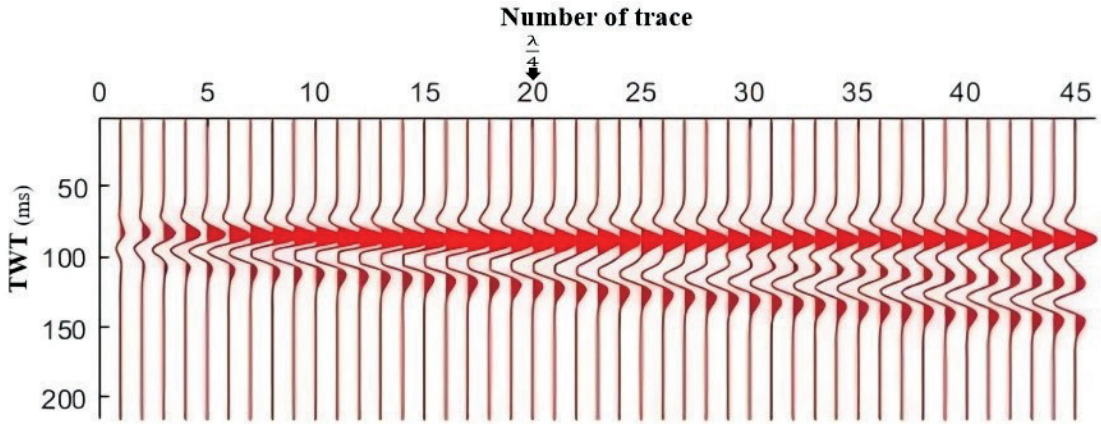

Fig. 14 - Synthetic seismic traces using a Ricker wavelet resulting from the synthetic model (Fig. 13). Trace number 20, which corresponds to the one-quarter wavelength thickness for the wedge model, is marked with an arrow in this figure.

Figs. 15 and 16 show the effectiveness of applying both the conventional and fast sparse ST attributes in detecting a wedge-shaped reservoir, synthetic model (Fig. 13).

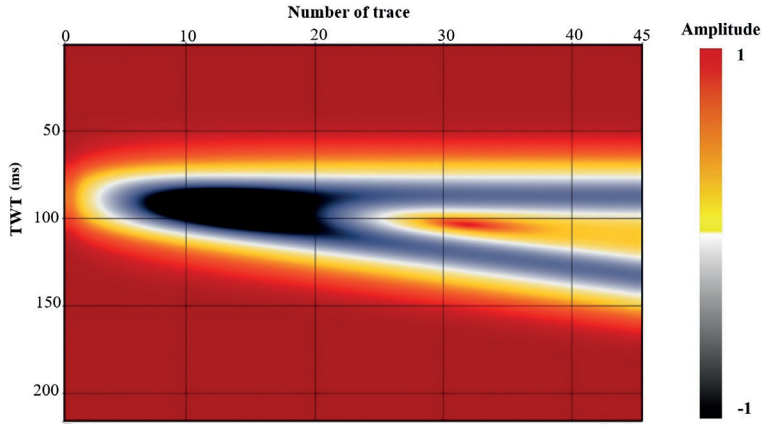

Fig. 15 - The conventional ST result in detecting a wedge-shaped reservoir, a synthetic model (Fig. 13).

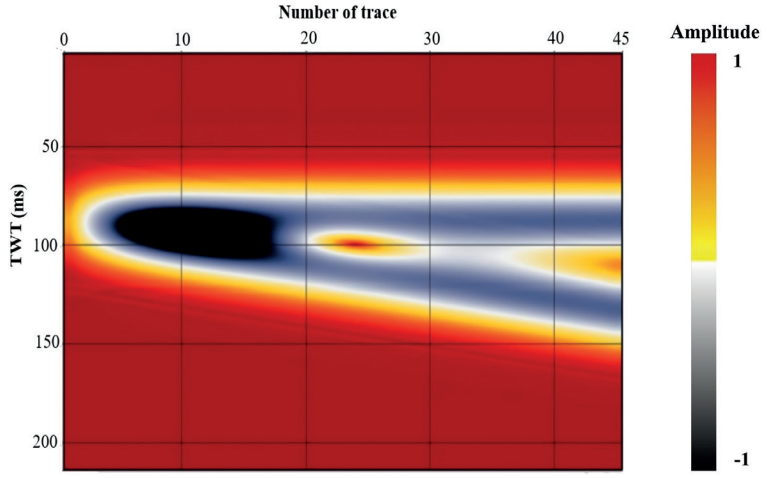

Fig. 16 - The fast sparse ST result in detecting a wedge-shaped reservoir, synthetic model (Fig. 13).

Though both attributes could have detected the synthetic wedge-shaped reservoir model (Fig. 13), it is evident that the resolution of the obtained model using fast sparse ST (Fig. 16) shows a better resolution than the model obtained using the formal ST (Fig. 15).

3. Results

We apply the frequency attributes to 3D seismic data from the Marun hydrocarbon field. Marun oil field is located in Zagros Basin, SW Iran. The neighbouring oil fields include Aghajari, Ahwaz, and Kupal. Marun oil field surface outcrop is the Aghajari Formation and Asmari, Bangestan and Khami are the three reservoirs in this oilfield. This oil field has 3-horizon reservoirs, which in ascending stratigraphical order are Asmari Formation, Bangestan, Gas, and oil-bearing reservoir, and Khami Group, a gas-bearing reservoir. This structure has 67 km length and 7 km thickness. It is situated 30 to 110 km SW of Ahvaz. The Asmari Formation with six reservoir

layers is the major oil reservoir of this field. In addition, it is mainly composed of carbonate units (limestone and dolomite). It is believed that the Asmari Formation has a good fracturing system in its first layer (more than 90% dolomite). The lithology of the Asmari reservoir is carbonate, shale, and sandstone and the lithology of Bangestan and Khami reservoirs is carbonate and shale. Due to tectonic activity, high fracture areas exist in this oil field, which causes upward migration of hydrocarbon (Shayesteh, 2002). The reservoir's depth for the Asmari Formation is from 2972 to 3212 m, also the average thickness is about 250 m but this thickness has changed from the east to the west. This field is an asymmetric anticline oriented NW-SE. The dimensions of the Marun oil field at the Asmari oil reservoir horizon are 67 and 7 km in length and thickness, respectively. Asmari oil reservoir is divided into 8 sectors. To date, 370 wells have been drilled in the Marun oil field. Except for 6 wells of Khami and 20 wells of Bangestan reservoirs, all wells were completed in the Asmari oil reservoir of this field. Fig. 17 shows the schematic cross-view of formations in the Marun oil field, and also a 3D view of the Asmari reservoir (Telmadarreie *et al*., 2012).

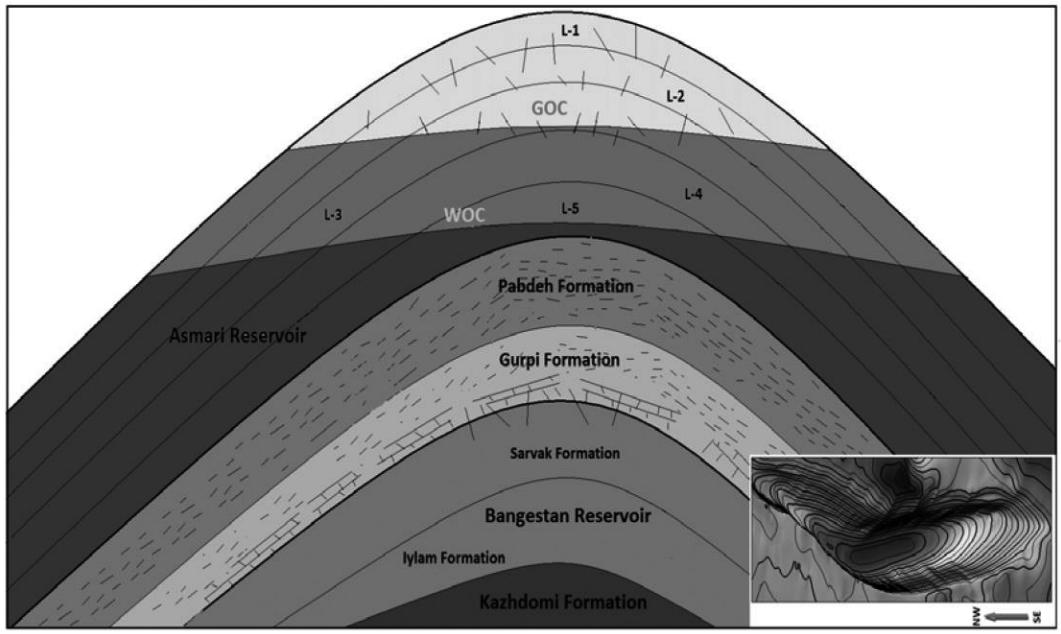

Fig. 17 - Scheme of the Asmari and Bangestan reservoirs section and the 3D view of the Asmari oil reservoir in the Marun oil field (Telmadarreie *et al.*, 2012).

Frequency perusal is a state-of-the-art and promising direction in geophysics and hydrocarbon exploration using seismic frequency information (Huang *et al*., 2020). Furthermore, the frequency responses and their measurements are not the main criteria for a good hydrocarbon reservoir so it is vital to combine other pieces of evidence like well-logs and extract appropriate seismic spectral decomposition features. Before extracting the spectral decomposition feature, the amplitude spectrum has been extracted for the seismic information as shown in Fig. 18. In Fig. 18, the maximum frequency of the seismic information is around 20 Hz, and the frequency band is from 0 to 18 Hz.

Due to the complexity of geological structures and several reflectors, data are not represented in 3D sections. Only in-line and cross-line are displayed in Figs. 19 and 20.

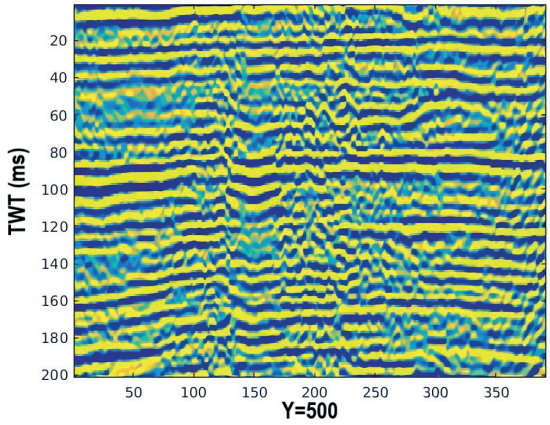

Fig. 19 - A 2D stacked in-line section selected from a 3D cube of the Marun oil field. Clear reflectors, from left to right on the vertical axis, are seen in this section, some of these reflectors are deflected in the y-axis range (82 to 123 ms).

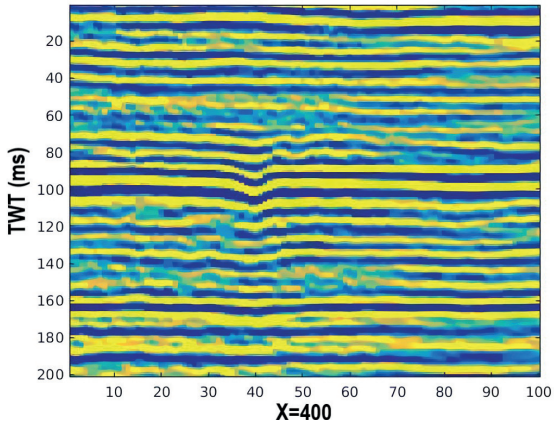

Fig. 20 - A 2D stacked cross-line section selected from a 3D cube of the Marun oil field. Clear reflectors, from left to right on the vertical axis, are seen in this section, some of these reflectors are deflected in the y-axis range (82 to 123) ms.

Time-frequency attribute, with corresponding frequencies of 20 Hz is obtained using fast sparse time-frequency transform and the results are shown in Figs. 21 and 22, respectively. The red arrows indicate the reflector's thickness variations in these seismic sections.

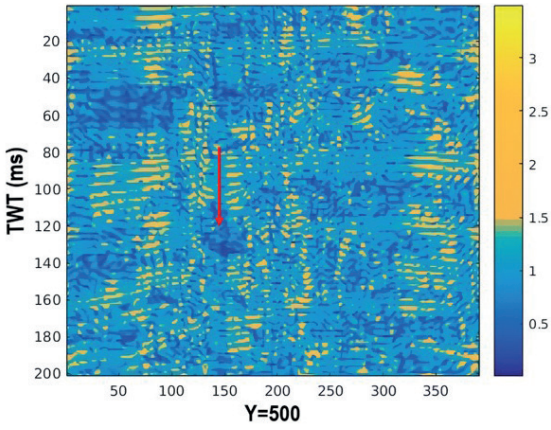

Fig. 21 - Analysing the frequency attribute of the in-line extracted image from a 3D seismic section, the Marun oilfield. The red arrow indicates the probable reflector's thickness variations in this time-frequency section.

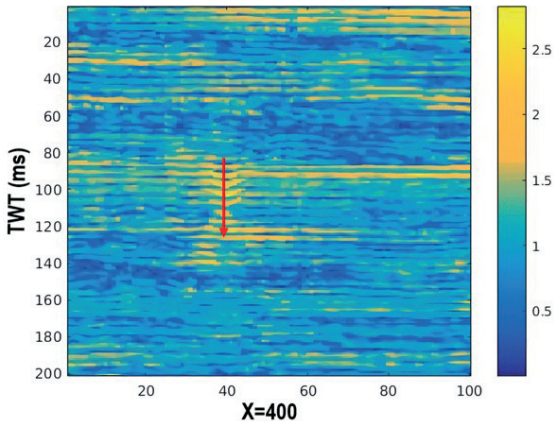

Fig. 22 - Analysing the frequency attribute of the cross-line extracted from a 3D seismic section, the Marun oilfield. The red arrow indicates the reflector's thickness variations in this time-frequency section.

It is evident that red arrows distinguish variations in thickness that can be considered as anomalies.

To check the reliability of the predicted results and the effectiveness of the proposed method, we examined the performances of both the instantaneous amplitude and fast sparse ST attributes in terms of frequency analysis of the reservoir interval versus thickness and amplitude. It is evident that, one of the most important issues in hydrocarbon reservoir characterisation is

predicting the thickness of hydrocarbon reservoirs by evaluating the frequency analyses and amplitude of seismic data in the reservoir interval. In this regard, instantaneous amplitude and fast sparse ST attributes are used on stacked seismic sections to evaluate the performances of both attributes in the prediction of the thickness of the reservoir interval. In this context, different analyses such as frequency versus thickness variations and frequency versus amplitude variations (Ortiz Bustos *et al.*, 2020) were performed. Fig. 23 shows the frequency range from 20 to 30 Hz versus 82 to 123 ms reservoir interval to evaluate the frequency variations versus thickness in the time domain.

In terms of validation, the results shown in Fig. 23 are compared with the obtained thickness of a well-log selected from the reservoir interval (Table 1).

Table 1 - The evaluated reflectors' thickness in the time domain and lithological information of the Asmari Formation from well logs.

Formation	Time interval (ms)	Lithology
Top of the reservoir	82	Carbonate
Base of the reservoir	123	Carbonate to Marl

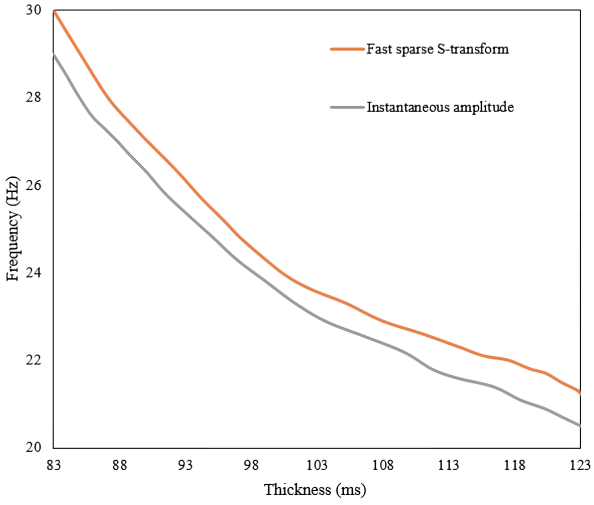

Fig. 23 - The frequency versus thickness variations using instantaneous amplitude and fast sparse ST. Note that the performance of the ST is superior to the instantaneous amplitude in the reservoir interval.

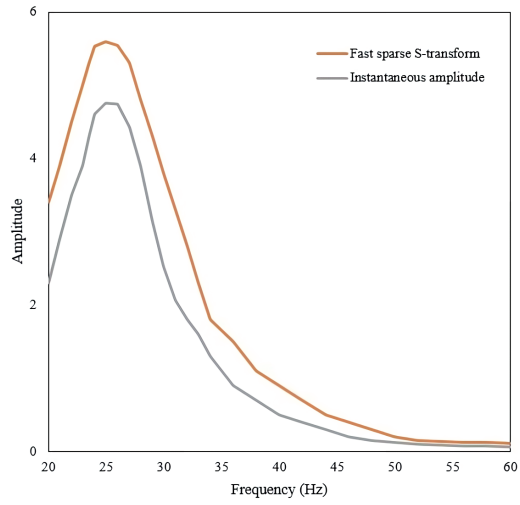

Fig. 24 - The amplitude versus frequency variations using instantaneous amplitude and fast sparse ST. The fast sparse ST has provided better performance than the instantaneous amplitude in the reservoir interval.

Fig. 24 shows the frequency range from 20 to 60 Hz versus amplitude to evaluate the frequency variations versus amplitude in reservoir intervals. The results show better performance of the fast sparse ST attribute compared to the instantaneous attribute. It is evident that the frequency span of the fast sparse ST attribute shows a better performance than the instantaneous amplitude.

4. Conclusions

In this study, the application of the instantaneous amplitude and of fast sparse ST attributes were examined to identify the local effects of reflectors and analyse the corresponding frequency spectrum applicable to reservoir characterisation. We analysed these methods to estimate the location and thickness of channel-shaped and wedge-shaped synthetic models, as well as experimental field data of a hydrocarbon reservoir. We found that the frequency content of the studied data is sensitive to the variation of reservoir thickness. There is a repetitive trend in the frequency spectrum, increasing with the thickness of the reservoir layer. Reflected waves from the bottom of layers with different thicknesses have different frequency and amplitude contents. Thus, the time-frequency cross-plot can be a suitable tool for identifying anomalies in thin layers forming hydrocarbon reservoirs. We conclude that the instantaneous amplitude attribute is ideal for predicting the synthetic models; however, the fast sparse ST resulted in better delineation of the synthetic models and field channel-shaped hydrocarbon reservoirs.

Acknowledgments. This research did not receive any specific grant from funding agencies in the public, commercial, or not-for-profit sectors. We thank the editors and four anonymous reviewers for their careful reviews and constructive comments. The second author would like to acknowledge the research council of the University of Tehran.

REFERENCES

Allen J.B. and Rabinar L.R.; 1977: *A unified approach to short-time Fourier analysis and synthesis*. Proc. IEEE, 65, 1558-1564, doi: 10.1109/proc.1977.10770.

Ashtari A. and Arzani A.; 2016: *Seismic spectral decomposition and inversion for buried channels delineation: a case study from the Asmari reservoir, southwestern Iran*. First Break, 34, 49-53.

Badly M.E.; 1985: *Practical seismic interpretation*. Prentice Hall Professional Technical Reference, Hoboken, NJ, USA, 266 pp.

Barnes A.E.; 1993: *Instantaneous frequency and amplitude at the envelope peak of a constant-phase wavelet.* Geophys., 56, 1058-1060.

Barnes A.E.; 2007: *A tutorial on complex seismic trace analysis.* Geophys., 72, W33-W43, doi: 10.1190/1.2785048.

Bourguignon B., Carfantan H. and Idier J.; 2007: *A Sparsity-Based method for the estimation of spectral lines from irregularly sampled data*. IEEE J. Sel. Top. Sign. Proces., 1, 575-585, doi: 10.1109/JSTSP.2007.910275.

Castagna J.P., Sun S. and Siegfried R.W.; 2003: *Instantaneous spectral analysis: detection of low-frequency shadows associated with hydrocarbons.* The Leading Edge, 22, 120-127.

Chakraborty A. and Okaya D.; 1995: *Frequency-time decomposition of seismic data using wavelet-based methods.* Geophys., 60, 1906-1916.

Chopra S. and Marfurt K.J.; 2006: *Seismic attribute mapping of structure and stratigraphy.* Society of Exploration Geophysicists, SEG/EAGE Distinguished Instructor Short Course 2006, Tulsa, OK, USA, 268 pp.

Chopra S. and Marfurt K.J.; 2007: *Seismic attributes for prospect identification and reservoir characterisation.* Society of Exploration Geophysicists, Tulsa, OK, USA, 464 pp., doi: 10.1190/1.9781560801900.

Chuang H. and Lawton D.C.; 1995: *Frequency characteristics of seismic reflections from thin beds.* Can. J. Explor. Geophys., 31, 32-37.

Ehirim C.N. and Akpan A.S.; 2017: *Continuous wavelet transform based spectral decomposition of 3D seismic data for reservoir characterisation in Oyi field, SE Niger Delta.* Am. J. Appl. Sci., 14, 766-771.

Gabor D.; 1946: *Theory of communication.* Journal of the Institution of Electrical Engineers, 93, 429-441.

Guo Q., Ba J., Luo C. and Xiao S.; 2020: *Stability-enhanced prestack seismic inversion using hybrid orthogonal learning particle swarm optimisation.* J. Pet. Sci. Eng., 192, 107313, doi: 10.1016/j.petrol.2020.107313.

Huang G., Bai M., Wang H., Liu X. and Chen Y.; 2020: *Frequency-space-dependent smoothing regularised nonstationary predictive filtering.* IEEE Trans. Geosci. Remote Sens., 60, 5902209, doi: 10.1109/TGRS.2021.3064945.

Jeong I.Y., Kim B. and Park H.M.; 2013: *Single-channel speech dereverberation based on non-negative blind deconvolution and prior imposition on speech and filter.* In: Proc. 20th International Conference on Neural Information Processing, ICONIP 2013, Daegu, Korea, pp. 469-476.

Liu J.; 2006: *Spectral decomposition and its application in mapping stratigraphy and hydrocarbons*. Ph.D. Thesis in Philosophy, Department of Geosciences, University of Houston, Houston, TX, USA, 128 pp.

Luo C., Ba J., Carcione J.M., Huang G. and Guo Q.; 2020: *Joint PP and PS pre-stack seismic inversion for stratified models based on the propagator matrix forward engine.* Surv. Geophys., 41, 987-1028, doi: 10.1007/s10712-020-09605-5.

Marfurt K.J. and Kirlin R.L.; 2001: *Narrow-band spectral analysis and thin-bed tuning.* Geophys., 66, 1274-1283.

Oluwadare O.A., Olowokere M.T., Taoili F., Enikanselu P.A. and Abraham-Adejumo R.M.; 2020: *Application of time-frequency decomposition and seismic attributes for stratigraphic interpretation of thin reservoirs in "Jude Field", offshore Niger delta.* AIMS Geosci., 6, 378-396, doi: 10.3934/geosci.2020021.

Ortiz Bustos V., Abarca-del-Río R., Belmonte-Pool A. and Miller M.; 2020: *Evaluation of thickness estimation techniques in seismically thin beds.* Obras y Proyectos, 28, 6-11, doi: 10.4067/S0718-28132020000200006.

Othman A., Fathy M. and Maher A.; 2016: *Use of spectral decomposition technique for delineation of channels for solar gas discovery, offshore west Nile delta, Egypt*. Egypt. J. Pet., 25, 45-51.

Partyka G., Gridley J. and Lopez J.; 1999: *Interpretational applications of spectral decomposition in reservoir characterisation.* The Leading Edge, 18, 353-360.

Raef A., Totten M., Vohs A. and Linares A.; 2017: *3D Seismic reflection amplitude and instantaneous frequency attributes in mapping thin hydrocarbon reservoir lithofacies: Morrison NE field and Morrison field, Clark County, KS*. Pure Appl. Geophys., 174, 4379-4394, doi: 10.1007/s00024-017-1664-1.

Sattari H.; 2017: *High-resolution seismic complex trace analysis by adaptive fast sparse S-transform.* Geophys., 82, V51-V67.

Shayesteh M.; 2002: *Investigation of hydrogen sulfide contamination of Asmari reservoir in Marun oil field.* In: Report 5207, National Iranian South Oil Company, Geology Department, Ahwaz, Iran, pp. 63-74.

Stockwell R.G.; 2007: *A basis for efficient representation of the S-transform.* Digital Signal Process., 17, 371-393.

Tanner M.T., Koehler F. and Sheriff R.E.; 1979: *Complex seismic trace analysis.* Geophys., 44, 1041-1063.

Telmadarreie A., Shadizadeh S.R. and Alizadeh B.; 2012: *Investigation of hydrogen sulfide oil pollution source: Asmari oil reservoir of Marun oil field in the southwest of Iran.* Iran. J. Chem. Eng., 9, 63-74.

Van Buchem F., Allan T., Laursen G., Lotfpour M., Moallemi A., Monibi S., Motiei H., Pickard N., Tahmasbi A. and Vedrenne V.; 2010: *Regional stratigraphic architecture and reservoir types of the Oligo-Miocene deposits in the Dezful Embayment (Asmari and Pabdeh Formations) SW Iran.* Geological Society London, Special Publication, 329, 219-263.

Widess M.B.; 1973: *How thin is a thin bed.* Geophys., 38, 1176-1180.

Yan T., Yang J., Liu Z. and Peng A.; 2018: *Application of instantaneous amplitude gradient for ground-penetrating radar signal analyses.* Arabian J. Geosci., 11, 636, doi: 10.1007/s12517-018-4000-x.

Zeng H.; 2010: *Geologic significance of anomalous instantaneous frequency.* Geophys., 75, P23-P30, doi: 10.1190/1.3427638.

Zheng X., Li Y., Li J. and Yu X.; 2007: *Reef and shoal reservoir characterisation using paleogeomorphology constrained seismic attribute analysis.* In: Expanded Abstracts 77th SEG International Exposition and Annual Meeting, San Antonio, TX, USA, pp. 1382-1386, doi: 10.1190/1.2792757.

Zhou X., Ba J., Santos E.J., Carcione M.J., Fu L.Y. and Pang M.; 2021: *Fluid discrimination in ultra-deep reservoirs based on a double double-porosity theory.* Front. Earth Sci., 9, 649984, doi: 10.3389/feart.2021.649984.

Corresponding author: Mohammad Ali Riahi
Institute of Geophysics, University of Tehran
North Krgar Ave., Tehran, Iran
Phone: +98 216 1118219; e-mail: mariahi@ut.ac.ir